

Redox-Active Sites in *Auricularia auricula-judae* Dye-Decolorizing Peroxidase and Several Directed Variants: A Multifrequency EPR Study

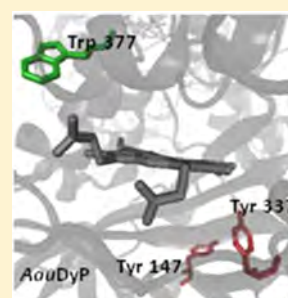
Maria Camilla Baratto,[†] Adalgisa Sinicropi,[†] Dolores Linde,[‡] Verónica Sáez-Jiménez,[‡] Lorenzo Sorace,[§] Francisco J. Ruiz-Duenas,[‡] Angel T. Martinez,[‡] Riccardo Basosi,[†] and Rebecca Pogni^{*,†}

[†]Department of Biotechnology, Chemistry and Pharmacy, University of Siena, I-53100 Siena, Italy

[‡]Centro de Investigaciones Biológicas, CSIC, Ramiro de Maeztu 9, E-28040 Madrid, Spain

[§]Department of Chemistry, "Ugo Schiff" and INSTM RU, University of Florence, 50019 Sesto Fiorentino, Florence, Italy

ABSTRACT: Peroxide-activated *Auricularia auricula-judae* dye-decolorizing peroxidase (DyP) forms a mixed Trp377 and Tyr337 radical, the former being responsible for oxidation of the typical DyP substrates (Linde et al. *Biochem. J.*, **2015**, 466, 253–262); however, a pure tryptophanyl radical EPR signal is detected at pH 7 (where the enzyme is inactive), in contrast with the mixed signal observed at pH for optimum activity, pH 3. On the contrary, the presence of a second tyrosine radical (at Tyr147) is deduced by a multifrequency EPR study of a variety of simple and double-directed variants (including substitution of the above and other tryptophan and tyrosine residues) at different freezing times after their activation by H₂O₂ (at pH 3). This points out that subsidiary long-range electron-transfer pathways enter into operation when the main pathway(s) is removed by directed mutagenesis, with catalytic efficiencies progressively decreasing. Finally, self-reduction of the Trp377 neutral radical is observed when reaction time (before freezing) is increased in the absence of reducing substrates (from 10 to 60 s). Interestingly, the tryptophanyl radical is stable in the Y147S/Y337S variant, indicating that these two tyrosine residues are involved in the self-reduction reaction.



INTRODUCTION

Dye-decolorizing peroxidases (DyPs) are a large and widely distributed heme peroxidase family found in fungi, bacteria, and archaea. DyPs share common structural characteristics with chlorite dismutases and other DyP-type related proteins, such as *Escherichia coli* EfeB, forming the CDE superfamily.^{1–5} The term “dye-decolorizing” derives from the ability of these enzymes to decolorize and degrade xenobiotic anthraquinone and azo dyes.^{6,7} The natural substrates of DyPs remain to be clarified even if an environmental role in lignin (and lignin products) biodegradation is suggested.^{8,9}

The fungal DyPs from *Bjerkandera adusta* and *Auricularia auricula judae* (*AauDyP*) were crystallized and biochemically characterized as representative for DyPs of two phylogenetically different basidiomycetes.^{1,10–15} The *AauDyP*, at first isolated and characterized from a fungal culture,¹⁶ has been recently overexpressed in *Escherichia coli* as inclusion bodies, and a refolding protocol has been optimized to obtain a recombinant protein with the same properties of wild DyP.¹⁷

The catalytic cycle of DyPs is similar to that of classical peroxidases, where the resting enzyme (with ferric heme) undergoes a two-electron oxidation by H₂O₂ to Compound I (oxo-ferryl heme with a porphyrin π -cation radical). The activated enzyme is then reduced back by two substrate molecules to the resting state via the so-called Compound II.¹⁸ Different than other fungal peroxidases, in the distal side of the heme plane of DyPs, arginine and aspartic residues (*AauDyP* Asp168 and Arg332) contribute to the heterolytic cleavage of

H₂O₂ to form Compound I in place of distal histidine and arginine residues commonly present in peroxidase-catalases. Both residues are required for H₂O₂ activation of *AauDyP*, as was demonstrated by the loss of enzyme activity after D168N and R332L single mutations.¹⁵

Long-range electron-transfer (LRET) routes from redox-active amino acids at the enzyme surface were reported in *Phanerochaete chrysosporium* lignin peroxidase (LiP) and *Pleurotus eryngii* versatile peroxidase (VP) and subsequently identified in the sequences of many putative LiPs and VPs from genomes of lignin-degrading white-rot basidiomycetes.^{19–21} To oxidize bulky substrates, a LRET pathway from radical forming amino acids was also suggested for the *AauDyP*.^{13,22}

AauDyP possesses seven Tyr and four Trp residues as potential sites to activate different LRET pathways (Figure 1).

This high number of Tyr residues in all basidiomycete DyPs²³ distinguishes them from ligninolytic peroxidases, like LiPs or VPs, in that they have none or only few tyrosines in their amino acid sequence.²⁴ Ligninolytic peroxidases oxidize lignin polymer and xenobiotic dyes at an exposed protein radical, mainly a Trp residue.^{25–28} An exception is represented by *Trametes versicolor* LiP that uses an exposed Tyr as the catalytic site, but it requires the formation of a reactive adduct

Special Issue: Wolfgang Lubitz Festschrift

Received: March 27, 2015

Revised: June 23, 2015

Published: June 29, 2015

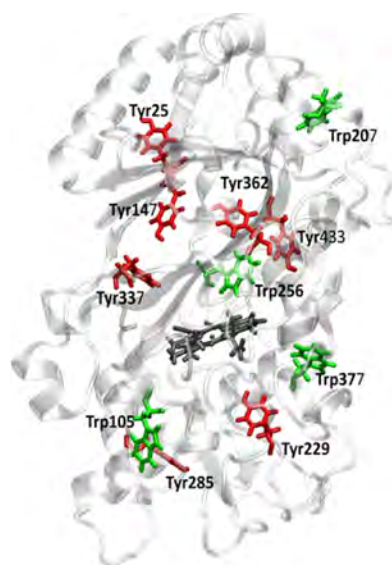


Figure 1. Heme prosthetic group (gray), Trp (green), and Tyr (red) residues in *AauDyP* (4W7J pdb code).

with veratryl alcohol.²⁹ This latter is the only case, to our knowledge, where a Tyr is involved in peroxidase catalysis. Usually the formation of Tyr radicals in peroxidases is indicative of enzyme oxidative inactivation.^{24,30}

In a recent paper, Protein Energy Landscape Exploration (PELE) simulations were performed to identify the possible substrate binding site(s) on the surface of the *AauDyP*, followed by EPR and directed mutagenesis studies.¹⁵ Three solvent-exposed residues (Trp377, Tyr337, and Tyr147) were selected as possible substrate oxidation sites. At pH 3, a mixed Trp377/Tyr337 radical was identified by the EPR technique, and kinetic measurements showed that the high turnover catalytic site is represented by the Trp377 residue. The catalytic activity on a typical substrate as Reactive Blue 19 is practically unaffected after substitution of Tyr337 by serine (k_{cat} 220–240 s^{-1}), while a strong decrease was observed after substituting Trp377 by serine ($k_{\text{cat}} \approx 9 \text{ s}^{-1}$).

In the present paper, starting from the recently published results, the recombinant *AauDyP* (and several single and double site-directed variants at the previously mentioned tryptophan and tyrosine residues) have been analyzed to identify the secondary tyrosyl radical(s). The study was performed by combining multifrequency electron paramagnetic resonance (EPR) spectroscopy and quantum mechanics/molecular mechanics (QM/MM) computational approach at different pHs and sample freezing times (in the absence of added reducing substrates), the latter resulting in different radical self-reduction rates.

■ EXPERIMENTAL AND THEORETICAL METHODS

DyP and Site-Directed Variants Production. The mature *A. auricula-judae* DyP (isoform I) (GenBank accession no. JQ650250)¹⁶ coding sequence was synthesized by ATG:biosynthetics (Merzhausen, Germany). Native enzyme and site-directed variants were expressed in *E. coli*, activated in vitro and purified as previously described.¹⁷ DyP simple variants (W377S, Y147S, and Y337S) were produced by PCR using the pET23a-DyPI vector as template and primers containing the desired mutation.¹⁵ For double mutations

(Y147F/Y337F, W377S/Y147S, and W377S/Y337S), the mutated vector for the first mutation was used as template.

EPR Spectroscopy. Continuous-wave CW-EPR X-band (9.39 GHz) measurements were performed with a Bruker E500 Eleksys Series using the Bruker ER 4122SHQE cavity, equipped with an Oxford Instruments helium continuous flow cryostat (ESR900). W-band (94.17 GHz) experiments were recorded on a Bruker Eleksys E600 spectrometer, operating in continuous wave equipped with a 6T split-coils superconducting magnet (Oxford Instruments), using a continuous flow helium cryostat (CF93S, Oxford Instruments). The enzymatic reaction was carried out by adding H_2O_2 in a *AauDyP*/peroxide molar ratio 1:10, with a final concentration of 0.1 μM enzyme in tartrate buffer at pH 3 or in Tris buffer at pH 7. For the X-band measurements, the addition of H_2O_2 was done directly in a 3.5 mm EPR tube, and the reaction time before freezing was ~ 10 or 60 s. For the W-band measurements, the reaction time before sample freezing was ~ 60 s. EPR spectra simulations were performed by the Easyspin 4.5.5 software package using the “pepper” function.³¹

Computational Methods. Protein Setup. Initial structure for Compound I of DyP (pdb code: 4W7J; resolution 1.79 Å) was obtained from the Protein Data Bank. Results of PROPKA3.1³² runs were used, in combination with visual inspection, to assign the protonation states of all titratable residues (aspartic acid, glutamic acid, and histidine) at the experimental pH. Missing hydrogen atoms were added by the psfgen module of VMD, version 1.9.1.³³ The protonated system, with crystallographic water molecules, was neutralized with sodium and chlorine ions (0.15 M ionic strength) and fully solvated in a rectangular box ($82 \times 86 \times 104 \text{ Å}^3$) of TIP3P water molecules using the autoionize and solvate modules of VMD. Solvent boxes were created with a layer of at least 10 Å of water molecules around each protein atom ($\sim 14\,000$ water molecules).

Preparatory Force-Field Calculations. AMBER force field^{34–36} and TIP3P³⁷ water model were used for both pure MM and hybrid QM/MM calculations. All available force-field parameters and charges were taken from the parm99.dat library.³⁵ For the treatment of the heme cofactor, the published parameters for the six-coordinate heme (heme_all.db3) available from the Amber parameter database³⁸ were used. Partial atomic charges for the oxyferryl heme and the iron-coordinated His175 residue were determined at the B3LYP/6-31G* (LANL2DZ on Fe) level with Gaussian03 software package³⁹ using a restrained electrostatic potential (RESP) procedure (as shown in table S1 and scheme S1 of ref 40). The solvated systems were relaxed by performing classical energy minimization and molecular dynamics (MD) simulations with NAMD 2.9 code.⁴¹ The positions of the hydrogen atoms and solvent water molecules were first energy-minimized and equilibrated at 298 K and 1 atm for 1 ns with a time step of 1 fs. Electrostatic interactions were taken into account using the Particle Mesh Ewald (PME) method,⁴² and periodic boundary conditions (PBC) were applied. Then, further 10 ns equilibration was carried out in which even the protein side chains were left free to equilibrate. During the MD simulations, the coordinates of the heme cofactor and protein backbone atoms were kept fixed to the crystal structure. A snapshot at the end of the MD equilibration run was taken and energy minimized to be used as starting structure for the following QM/MM computations.

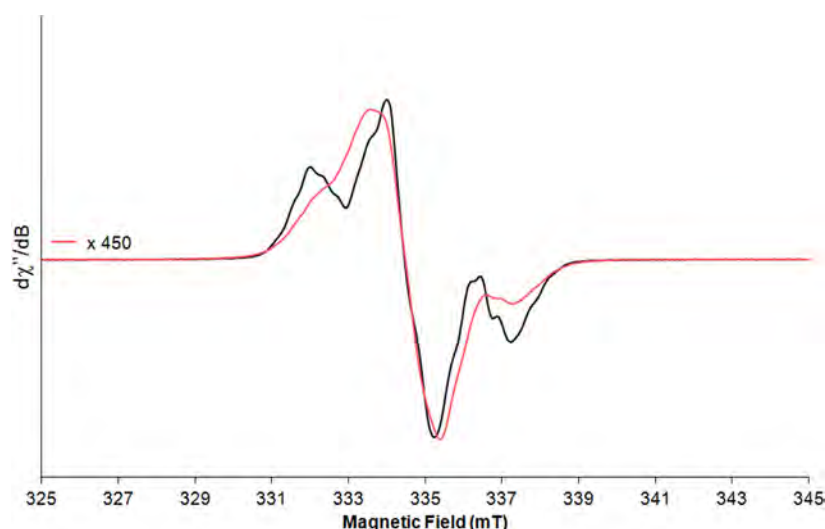


Figure 2. 40 K narrow scan X-band EPR spectra of radical species formed in *AauDyP* at pH 3 after the addition of 10 equiv H_2O_2 and rapid (10 s) freezing (black line) and after a reaction time of 60 s (red line). Experimental conditions: $\nu = 9.39$ GHz, 0.2 mT modulation amplitude, 0.2 mW microwave power.

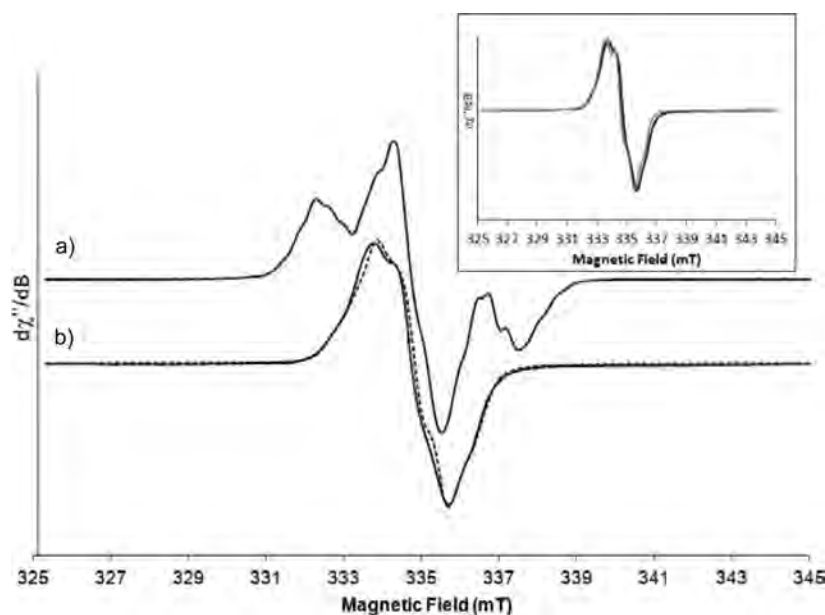


Figure 3. 40 K narrow scan X-band EPR spectra of protein radical species at pH 3 in (a) *AauDyP* and in (b) *W377S/Y147S* variant paired with its simulation. Inset: 40 K narrow scan X-band EPR spectra of the radical intermediate in the *W377S/Y147S* double variant (black line) and the *W377S* variant (gray line). Experimental conditions: $\nu = 9.39$ GHz, 0.2 mT modulation amplitude, 0.5 mW microwave power.

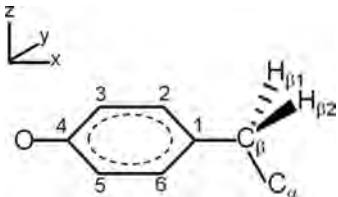
QM/MM Calculations. All QM/MM calculations were performed with the MOLCAS 7.4 package⁴³ coupled with a modified version of the MM package Tinker 4.2.⁴⁴ An electronic embedding (EE) scheme was applied, using hydrogen link atoms (HLA) with a scaled-charge model to treat the QM/MM boundary region. The present QM/MM protocol has already been successfully applied in previous works.^{40,45–47} Trp377, Tyr337, and Tyr147 radicals were simulated in the deprotonated/neutral forms. QM/MM geometry optimizations were performed at the B3LYP/AMBER level using the 6-31G* basis set. The Morokuma's scheme as implemented in MOLCAS 7.4⁴³ was applied to constraint the LA position on the line connecting the QM and the MM atoms.

EPR Computations. EPR magnetic parameters (g tensors, $hfcc$'s, and Mulliken spin densities) have been computed via single-point calculations on the B3LYP/AMBER-optimized structures using the ORCA2.9 program package⁴⁸ with an EE scheme, in which fixed MM point charges are included in the one-electron QM Hamiltonian and the QM/MM electrostatic interactions are evaluated from the QM electrostatic potential and the MM charges. In these calculations, the B3LYP^{49–51} functional was used in combination with the Barone's EPRII basis set.⁵²

RESULTS AND DISCUSSION

X-Band EPR Spectra of *AauDyP* and Its Tryptophan and Tyrosine Variants. Previous EPR characterization showed that the ferric species in the recombinant *AauDyP*

Table 1. Experimental (pH 3) and B3LYP/EPR-II g Tensors (g_i) and hfcc Values (A_i , in MHz) Computed at the B3LYP/AMBER-Optimized Geometries for Tyr337[•] and Tyr147[•]



		g_i^a	$A_i(H_{\beta 1})$	$A_i(H_{\beta 2})$	$A_i(H_2)$	$A_i(H_6)$	$A_i(H_3)$	$A_i(H_5)$	
sim.									
W377S/Y147S	x	2.0075	16.6	15.4	2.0	2.7	26.0	24.0	
	y	2.0043	17.3	16.0	4.5	5.2	21.0	19.0	
	z	2.0020	22.4	21.0	8.1	9.0	7.0	7.0	
comp.	iso	2.0046	18.8	17.5	4.9	5.6	18.0	16.6	
	Tyr-337 [•]	x	2.0066	16.6	15.4	2.0	2.7	-6.6	-5.7
		y	2.0043	17.3	16.1	4.5	5.2	-20.3	-18.7
		z	2.0022	22.4	21.5	8.1	9.0	-26.3	-24.2
comp.	iso	2.0044	18.8	17.7	4.9	5.6	-17.8	-16.2	
	Tyr-147 [•]	x	2.0093	42.7	-0.5	4.4	4.3	-8.5	-7.6
		y	2.0047	43.7	-0.9	6.6	6.3	-23.2	-21.3
		z	2.0023	48.7	4.7	11.2	10.9	-30.4	-27.9
iso	2.0054	45.0	2.0	7.4	7.2	-20.7	-18.9		

^a g_x value has been measured from the 94 GHz EPR spectrum. The errors on the g values are ± 0.0001 for g_x and ± 0.0002 for g_y and g_z . Although the agreement with the experimental g_x value is not satisfactory, the computed g tensor values clearly indicate that the two Tyr radicals (Tyr337[•] and Tyr147[•]) are embedded in a contrasting hydrogen-bonding status and protein electrostatic environment and that only in the case of Tyr337[•] the parameters are compatible with a residue present in a strongly H-bonded environment that is in accord with the experiments.

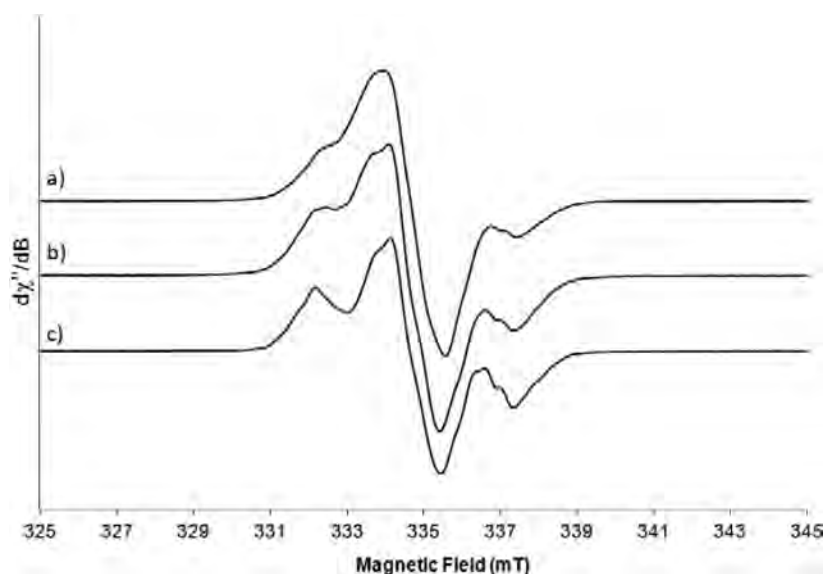


Figure 4. 40 K narrow scan X-band EPR spectra of radical species at pH 3 in the Y147S (a), Y337S (b), and Y147F/Y337F (c) variants after H_2O_2 activation and 60 s reaction time before freezing. Experimental conditions: $\nu = 9.39$ GHz, 0.2 mT modulation amplitude, 0.5 mW microwave power. The EPR spectra are normalized in intensity.

resting state is predominately in its axial spin state, $g_{\perp} \approx 6$ and $g_{\parallel} = 2.0$, while in the H_2O_2 -activated enzyme the iron signal disappears and an intense protein radical signal is evident.¹⁵ In Figure 2, the narrow scan of the EPR spectrum obtained after H_2O_2 activation with freezing time less than 10 s is compared with that recorded after 60 s freezing time. As already reported, the EPR signal at the shorter reaction time (black trace) showed the presence of a mixed Trp377/Tyr337 radical. The spectrum recorded at longer reaction time (red trace) is greatly decreased in intensity as the Trp radical signal quickly decays while the Tyr contribution becomes more evident.

Previous EPR and directed-mutagenesis studies of the W377S variant confirmed the assignment of the tryptophanyl radical species to Trp377 and its role as the high turnover catalytic site in *AauDyP*.¹⁵ The EPR spectrum of the double variant W377S/Y147S has been recorded and is reported here for the first time to rule out the involvement of Tyr147 residue as secondary radical species in native *AauDyP* (Figure 3). The spectrum of this variant has been simulated with the magnetic parameters reported in Table 1, and the experimental spectrum is superposed in the inset of Figure 3 to the one recorded for the W377S variant. The similarity of the W377S and W377S/

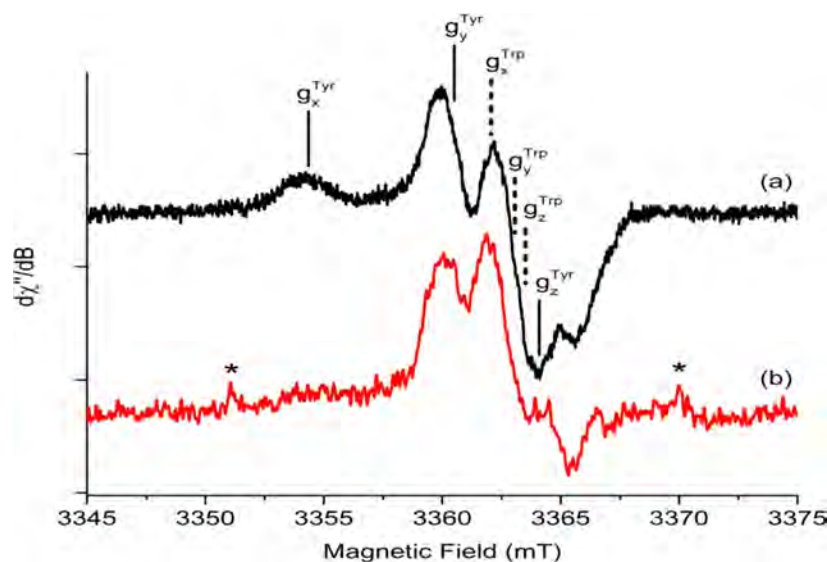


Figure 5. Narrow-scan W-band EPR spectra ($\nu = 94.2992$ GHz) recorded at 100 K of *AauDyP* (a) and of Y147F/Y337F variant (b) after H_2O_2 -activation and 60 s reaction time before freezing. The solid and dashed vertical lines evidence the position of the resonances of tyrosine and tryptophan radicals expected on the basis of theoretical calculations. (See Table 1.) Experimental conditions: modulation amplitude 0.1 mT; microwave power: 0.05 mW. The asterisks mark two unavoidable spurious signals originating from Mn(II) on cavity walls.

Y147S EPR spectra permits us to assign the secondary radical species to Tyr337 at pH 3 and to confirm that the Tyr147 is not contributing to the spectrum of *AauDyP*.

The principal LRET pathway starting from Trp377 in *AauDyP* is equivalent to that found in VPs^{25,26} and LiP,¹⁹ where a Trp catalytic site is involved. Trp377 is the candidate of choice for the oxidation of bulky substrates because it is very close to the heme moiety (7 Å from the cofactor), the nitrogen atom of the indole ring is solvent-exposed, and the pathway for the LRET to the heme is the shortest one. Interestingly, not only Trp377 but also the residues Pro310 and Arg306 in the electron-transfer pathway are conserved in sequences of many basidiomycete DyPs.^{15,23} Among the other tryptophans, Trp105 and Trp256 are solvent-exposed; however, the indole ring is not accessible for the oxidation of reducing substrates. Trp207 is solvent-exposed and can be oxidized, but as the electron coupling exponentially decays with the distance from the heme, Trp207 can be ruled out for its large distance from the heme moiety.

At longer reaction time the tyrosyl secondary radical contribution is more evident, as shown in Figure 4, where the EPR spectra of Y147S (a), Y337S (b) and Y147F/Y337F (c) at X-band, recorded after 60 s of reaction time, are reported. For Y147S and Y337S variants (Figure 4a,b) the EPR spectra show the superposition of a tyrosyl radical and the main contribution of the thryptophanyl radical species. The tyrosyl radical species can be assigned to Tyr337 and to Tyr147, respectively. Both of them are absent in the EPR spectrum of Y147F/Y337F double variant (Figure 4c). The latter is greatly reduced in intensity and shifted to lower g values compared with the EPR spectrum of native DyP. We point out that the EPR spectrum of the Y147S variant is identical to that recorded for native *AauDyP* at longer reaction time (Figure 2, red line), confirming the involvement of the only Tyr337 as the secondary radical species at the pH for optimum activity.

Interestingly, the self-reduction of the Trp377 neutral radical observed during (60 s) reaction of *AauDyP* with H_2O_2 , which resulted in an EPR signal dominated by the tyrosyl component (Figure 2), was not observed for the Y147F/Y337F variant,

which maintained the tryptophanyl radical line shape at the end of the reaction period (Figure 4c). This result together with those obtained for the single Y147S and Y337S variants, the former self-reducing as the wild-type enzyme (Figure 4a) while the second one seems to proceed with a lower reduction rate (Figure 4b), indicates that these two surface tyrosines are involved in Trp377 radical self-reduction. The mechanism of reduction of the catalytic tryptophanyl radical of *AauDyP*, in the absence of reducing substrates, remains to be established, but both enzyme intra- and intermolecular reactions could be produced.

W-Band EPR Spectra and QM calculations of *AauDyP* and Its Directed Variants. Radicals immobilized in proteins can be identified by their g -tensor values that are not affected by different geometries such as side chain orientations. The g tensor is a fingerprint of the particular type of radical, and it may be used to identify protein radical species when protein environments induce changes of the hyperfine structure.^{53–56} Tyrosine and tryptophan radicals are difficult to be distinguished at the X-band (9 GHz) EPR, whereas at W-band (94 GHz) they are clearly identified on the basis of the different anisotropy of the two species: much larger g_x and g_y tensor values are observed for tyrosyl radical exhibiting large spin density on oxygen compared with tryptophan radicals with spin densities on nitrogen or carbon atoms.⁵⁷ In this context, W-band EPR spectra of both native *AauDyP* and Y147F/Y337F variants have been recorded to unequivocally identify the protein radical species (Figure 5).

The spectra are recorded under the same experimental conditions (pH and reaction time) of the X-band spectra reported in Figure 4. The spectrum of the native DyP in Figure 5a shows the presence of contributions from two radical species with different g -tensor anisotropy, which were attributed to mixed Trp377/Tyr337 protein radical in ref 15. The possibility to compare the experimental results with the calculated g values (see later) for the different radicals allows us to confirm the assignment. Furthermore, the comparison with the W-band EPR spectrum of the double variant Y147F/Y337F points out the absence of the tyrosyl protein radical contribution. The

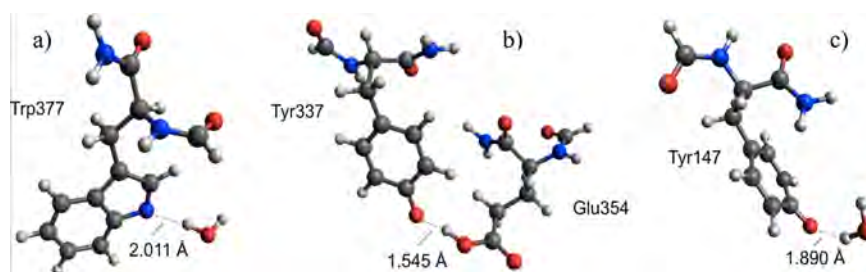


Figure 6. QM part of the B3LYP/AMBER optimized geometries for Trp377 (a), Tyr337 (b), and Tyr147 (c) radicals.

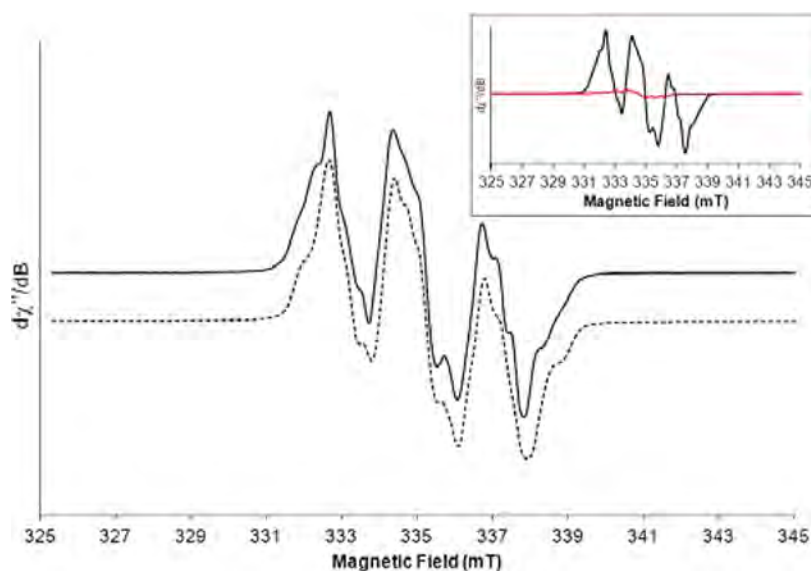


Figure 7. 40 K narrow scan X-band EPR spectrum of radical species at pH 7 in *AauDyP* (black line) after the addition of H_2O_2 and rapid freezing, compared with its simulation (dotted line). Inset: 40 K X-band EPR spectrum of the same radical (black line) and W377S variant (red line) at pH 7. Experimental conditions: $\nu = 9.39$ GHz, 0.2 mT modulation amplitude, 0.5 mW microwave power.

absence of any detectable signal from tyrosine residues in the double variant evidence that Tyr337 and Tyr147 are the only tyrosines (among the seven) forming a protein radical potentially involved in a LRET process. For a tryptophanyl radical, the field corresponding to 94 GHz EPR (3.3 T) still does not represent the so-called high-field limit, where the g -tensor shifts exceed the hyperfine splitting and the three g -tensor components are separated in the spectrum. Typical g -tensor values for tryptophan radicals are $g_x \approx 2.0033$ to 2.0035 , $g_y \approx 2.0024$ to 2.0025 , and $g_z \approx 2.0021$.⁵⁶ Only recently, the small g -tensor anisotropy for tryptophan radicals has been solved using an EPR spectrometer operating at 700 GHz.⁵⁸ The case is the opposite for tyrosine radicals for which the g -tensor components are well-separated at 94 GHz. It is well known, both from experimental⁵⁷ and theoretical studies,^{40,46,59,60} that the hydrogen-bonding status and protein electrostatic environment of tyrosine radicals can be evaluated from their g -tensor values. In particular, the g_x value is sensitive to even relatively weak electrostatic perturbations and especially to hydrogen bonds between the carbonyl group of tyrosine and the protein environment. The g_x values for tyrosine radicals range from 2.0065, due to a strong hydrogen bond, to 2.0094,⁵⁷ in a non-polar and non-hydrogen-bonding environment ($g_y \approx 2.0040$ to 2.0043 and g_z to 2.0021).

In *AauDyP* (Figure 5a), the g_x value of 2.0075 experimentally determined can be connected to an electropositive electrostatic effect of the environment. Indeed, such a low value of g_x can be

correlated with Tyr337, as it can arise from the strong hydrogen bond interaction between the phenoxyl oxygen and the phenoxyl proton transferred to the carboxylic oxygen of the nearby Glu354 residue (Figure 6b and Table 1).

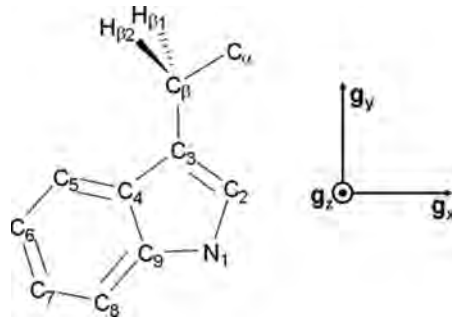
The role of such hydrogen bonds in lowering the g_x value is in agreement with previous works on tyrosine radicals: in particular, this effect has been evidenced also in the catalytic cycle of the *P. eryngii* VP variant following the Tyr164 protein radical formation.^{46,60} On the contrary, Tyr147 in *AauDyP* is involved in a weaker hydrogen bond with solvent water molecules (1.890 Å) (Figure 6c) that causes an increase in the g_x value (Figure 6c and Table 1). At the same time, the hf-tensor values of the side-chain β -protons of tyrosine radicals as well as those of tryptophan radicals dominate the EPR protein radical spectra.⁵³ The magnitude of the isotropic part (A_{iso}) of the hf-tensor of β -protons is a function of the spatial orientation of the side chain and is given by the McConnell relations²⁵

$$A_{\text{iso}}(\text{H-}\beta_1) = \rho_{\text{C3}}(B' + B'' \cos^2 \theta_1) \quad (1)$$

$$A_{\text{iso}}(\text{H-}\beta_2) = \rho_{\text{C3}}(B' + B'' \cos^2 \theta_2) \quad (2)$$

where B' and B'' are empirical constants ($B' = 0$, $B'' = 5$ mT)^{25,53,54} and θ_1 , θ_2 are the dihedral angles between the p_z axis (i.e., p_z orbital of C3) and the projected $\text{C}_\beta\text{-H}_{\beta 1,2}$ bonds. Because the crystal structure of the enzyme is present, a site-specific radical assignment can be made on the basis of the comparison of the experimental and crystallographic dihedral

Table 2. Experimental (*AauDyP* pH 7) and B3LYP/EPR-II g Tensors (g_i) and hfcc Values (A_i , in MHz) Computed at the B3LYP/AMBER-Optimized Geometries for Trp377^a



		g_i^a	$A_i(\text{H}_{\beta 1})^b$	$A_i(\text{H}_{\beta 2})$	$A_i(\text{H}_2)$	$A_i(\text{H}_3)$	$A_i(\text{H}_6)$	$A_i(\text{H}_7)$	$A_i(\text{N}_1)$	$A_i(\text{H}_1)$
sim.	x	2.0037	65.4	48.9		19.7		15.8	0.3	
Trp377 ^a	y	2.0027	47.3	42.5		25.6		5.3	18.5	
	z	2.0022	84.6	45.7		12.1		7.0	17.5	
	iso	2.0028	65.7	45.7		19.1		9.4	12.1	
	comp.	x	2.0037	77.4	37.2	-2.7	-13.1	0.7	-9.8	-2.1
Trp377 ^a	y	2.0028	74.9	35.8	0.0	-5.0	-0.3	-2.8	-1.9	-1.9
	z	2.0023	84.5	44.8	5.5	-15.9	3.3	-14.5	34.1	5.0
	iso	2.0029	78.9	39.2	0.96	-11.3	-1.2	-9.0	10.0	0.3

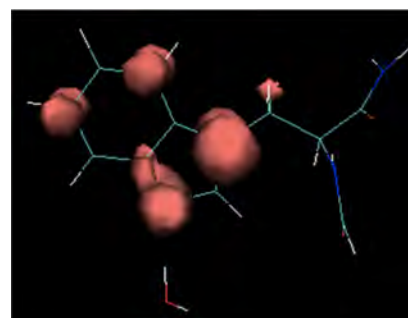
^aErrors on the simulated g_i values are ± 0.0001 . ^bhfcc values ± 6 MHz

angle values.²⁵ In Table 1, the computed magnetic parameters for Tyr337 and Tyr147 are reported and compared with the parameters obtained from the simulated spectrum of W377S/Y147S variant. The two Tyr residues have a different spatial orientation in the crystal structure, giving rise to different values of the hyperfine coupling constants for the two β -protons of the side chain (Table 1). The experimental and computed hyperfine coupling constants are consistent with the assignment to Tyr337 as the secondary radical species formed in *AauDyP* at pH 3; however, once the Tyr337 is removed, a potential LRET pathway originating from Tyr147 is activated. When both the Tyr residues are removed, no trace of tyrosyl radical contribution is present, as it is clear by the inspection of both the X-band (Figure 4c) and W-band (Figure 5b) EPR spectra of the Y147F/Y337F variant.

EPR Spectra of *AauDyP* at Neutral pH. Because *AauDyP* is catalytically inactive at pH 7, the EPR spectrum has been recorded to check the presence of protein radicals. The narrow scan of the EPR spectrum of the H_2O_2 -activated enzyme paired with its simulation is reported in Figure 7. The EPR spectrum of the W377S variant (red line) was recorded at the same pH and compared with the one of *AauDyP* to assign this tryptophanyl spectrum (Figure 7, inset). The Trp377 EPR signal disappears, leaving only a residual signal of another paramagnetic species almost undetectable, confirming the assignment of the radical species at pH 7 only to Trp377. The indole ring rotation angle, ϕ , defined by $\text{C}\alpha\text{-C}\beta\text{-C}3\text{-C}2$, is $\phi \approx -15^\circ$ for Trp337 (4W7J pdb code). The crystallographic dihedral angles for the β -protons are $\theta_1 \approx 130^\circ$ for H- $\beta 1$ and $\theta_2 \approx 140^\circ$ for H- $\beta 2$. The calculated values, considering $\rho_{\text{C}3} = 0.55(1)$ and $B'' = 5$, are $\theta_1 \approx 128^\circ$ for H- $\beta 1$ and $\theta_2 \approx 147^\circ$ for H- $\beta 2$, which are in fair agreement with the experimental and computed values reported in Tables 2 and 3.

It is interesting to note that at this pH the enzyme is catalytically inactive.²³ This can be due to a decrease in tryptophan redox potential in aqueous solution when the pH is increased.⁶¹

Table 3. B3LYP/EPR-II-Computed Mulliken Spin Densities for Trp377^{a,b}



	Trp377 ^a
N_1	0.28
C_2	-0.10
C_3	0.57
C_5	0.18
C_7	0.13

^aComputed spin density distributions of the radical species visualized with the program package VMD³³ is shown above the table. ^bTotal Mulliken spin density is equal to one adding the small contributions from the remaining QM atoms.

LRET Pathway/s in *AauDyP*. The first LRET pathway in ligninolytic peroxidases was identified in *P. chrysosporium* LiP.¹⁹ This pathway starts from the exposed Trp171 to the heme. The Trp radical, in its cationic form, was indirectly determined and represents the catalytic site for the oxidation of veratryl alcohol, which in turn oxidizes bulky substrates like the lignin polymer.¹⁹ A Trp cation radical was reported after engineering the Trp171 site in LiP and *Coprinus cinereus* peroxidase,⁶² but it was subsequently demonstrated that the detected Trp171 radical was in its neutral form.⁴⁷ Until now, the only case of a Trp cation radical (Trp191^{•+}) as a catalytic site is that detected in cytochrome *c* peroxidase (CcP) by Hoffmann et al.^{63–65} and recently confirmed by a computational study.⁴⁰

In *P. eryngii* VP, the catalytic site is the tryptophanyl neutral radical (Trp164[•]) H-bonded to N1 with the carboxylic group of the nearby Glu243 as the hydrogen bond donor.²⁵ The formation of the neutral tryptophan radical with the electron transfer followed by a proton transfer (ETPT) is consistent with the formation of a short-lived transient radical cation with a lifetime of few picoseconds.⁴⁶

The Trp377 radical in *AauDyP* is in its neutral form, with the indole ring solvent-exposed and water molecules as hydrogen bond donors (2.011 Å, Figure 6a). The *AauDyP* indole ring rotation angle ϕ , $\phi \approx -15^\circ$, is close to the same crystallographic angle for Trp164 in *P. eryngii* VP ($\phi \approx -22^\circ$).²⁵ Considering also a small reorientation, followed by protein radical formation, these two residues have very similar β -protons coupling constants and the same catalytic role in both proteins.

It is worth noting that a different line shape is observed in the EPR spectrum (pH 7) assigned to the “pure” neutral Trp377 radical (Figure 7) compared with that obtained (pH 3) for the Y147F/Y337F double variant (Figure 4c), where the secondary tyrosyl radical species are absent. The spectrum of the double variant, and consequently the tryptophanyl contribution in the EPR spectrum of native *AauDyP*, might be originated by the overlay of another Trp secondary radical species with the activation of the LRET pathway starting from Trp377. It has been shown that methionine residues play a role in the electrostatic stabilization of Trp protein radicals.^{47,25,62,66–68} Comparison of the crystal structures of *P. eryngii* VP²⁰ and *AauDyP*¹³ shows that a methionine residue (Met247) close to the Trp164[•] in the *P. eryngii* VP enzyme is replaced by two phenylalanine residues (Phe383 and Phe372) in Trp377[•] in *AauDyP*. The Met residues were proposed to contribute to the electrostatic stabilization of Trp191 cation radical also in CcP. Changing even two of the three Met residues in CcP to the corresponding residues in ascorbate peroxidase eliminates the Trp191 EPR signal and generates a Tyr-like EPR signal.^{67,68} It is also interesting that in *AauDyP* when the main LRET pathway is removed, the principal radical signal is that of a Tyr residue. The presence of the two Phe residues in *AauDyP* can play a role in the destabilization of the Trp377[•], delocalizing electron equivalents on other redox-active sites. The other two Trp residues of possible secondary tryptophanyl radical sites are Trp256 and Trp105. Trp256 is connected to the heme propionate group, while Trp105 is linked to Trp377 through a pathway starting from Trp105 \rightarrow Arg217 \rightarrow Phe370 \rightarrow Phe372 \rightarrow Trp377 and it is hydrogen bonded to Glu100. Studies are in progress to also address the involvement of an eventual secondary tryptophan radical contribution to the spectrum of *AauDyP* at pH 3.

CONCLUSIONS

In conclusion, in *AauDyP* at pH for optimum activity, the solvent-exposed catalytic site for the oxidation of bulky substrates is the Trp377 residue, which appears in its neutral form with the water molecules as hydrogen bond acceptors. A secondary radical is simultaneously formed: this is localized on Tyr337 that is hydrogen-bonded with Glu354. When the main LRET is removed in the W377S variant, the Tyr337 residue provides the main radical site. If the Tyr337 residue is removed in the Y337S variant, the Tyr147 radical, hydrogen-bonded to water molecules, becomes the secondary radical species. At pH 7, only the Trp377 radical is present.

The *AauDyP* can represent a nice example to study the mechanism that underlines the activation or deactivation of different LRET pathways in enzymatic systems. The possibility to tune the redox-active sites can be relevant for the use of this class of enzymes in biotechnological applications.

AUTHOR INFORMATION

Corresponding Author

*Tel: +39 0577 234258. E-mail: rebecca.pogni@unisi.it.

Notes

The authors declare no competing financial interest.

ACKNOWLEDGMENTS

This work was supported by the PRIN 2009-STNWX3 project of the Italian Ministry of Education, Universities and Research (MIUR), the HIPOP (BIO2011-26694) project of the Spanish Ministry of Economy and Competitiveness (MINECO), and the INDOX (KBBE-2013-7-613549) European project. F.J.R.-D. acknowledges a *Ramón y Cajal* contract of the Spanish MINECO. L.S. acknowledges the financial support of Ente Cassa di Risparmio di Firenze. Careful reading and revising of the manuscript by Professor Emeritus Les Brooks, Sonoma State University, is gratefully acknowledged.

ABBREVIATIONS

CDE, chlorite dismutase, DyP, and *E. coli* EfeB superfamily; DyP, dye-decolorizing peroxidase; EPR, electron paramagnetic resonance; LiP, lignin peroxidase; LRET, long-range electron transfer; VP, versatile peroxidase

REFERENCES

- (1) Kim, S. J.; Shoda, M. Purification And Characterization Of a Novel Peroxidase from *Geotrichum candidum* Dec 1 Involved in Decolorization of Dyes. *Appl. Environ. Microbiol.* **1999**, *65*, 1029–1035.
- (2) Sugano, Y. DyP-type Peroxidases Comprise a Novel Heme Peroxidase Family. *Cell. Mol. Life Sci.* **2009**, *66*, 1387–1403.
- (3) Hofrichter, M.; Ullrich, R.; Pecyna, M. J.; Liers, C.; Lundell, T. New and Classic Families of Secreted Fungal Heme Peroxidases. *Appl. Microbiol. Biotechnol.* **2010**, *87*, 871–897.
- (4) Ruiz-Dueñas, F. J.; Martínez, A. T. Structural and Functional Features of Peroxidases with a Potential as Industrial Biocatalysts. In *Biocatalysts Based on Heme Peroxidases*; Torres, E., Ayala, M., Eds.; Springer-Verlag: Berlin, 2010; pp 37–59.
- (5) Colpa, D. I.; Fraaije, M. W.; van Bloois, E. DyP-type Peroxidases: a Promising and Versatile Class of Enzymes. *J. Ind. Microbiol. Biotechnol.* **2014**, *41*, 1–7.
- (6) Sugano, Y.; Matsushima, Y.; Tsuchiya, K.; Aoki, H.; Hirai, M.; Shoda, M. Degradation Pathway of an Anthraquinone Dye Catalyzed by a Unique Peroxidase DyP from *Thanatephorus cucumeris* Dec 1. *Biodegradation* **2009**, *20*, 433–440.
- (7) Sugano, Y.; Matsushima, Y.; Shoda, M. Complete Decolorization of the Anthraquinone Dye Reactive Blue 5 by the Concerted Action of Two Peroxidases from *Thanatephorus cucumeris* Dec 1. *Appl. Microbiol. Biotechnol.* **2006**, *73*, 862–871.
- (8) Salvachúa, D.; Prieto, A.; Martínez, A. T.; Martínez, M. J. Characterization of a Novel Dye-Decolorizing Peroxidase (DyP)-Type Enzyme from *Irpex lacteus* and Its Application in Enzymatic Hydrolysis of Wheat Straw. *Appl. Environ. Microbiol.* **2013**, *79*, 4316–4324.
- (9) Yu, W.; Liu, W.; Huang, H.; Zheng, F.; Wang, X.; Wu, Y.; Li, K.; Xie, X.; Jin, Y. Application of a Novel Alkali-Tolerant Thermostable DyP-type Peroxidase from *Saccharomonospora viridis* DSM 43017 in Biobleaching of Eucalyptus Kraft Pulp. *PLoS One* **2014**, *9*, e110319.
- (10) Sugano, Y.; Muramatsu, R.; Ichiyanagi, A.; Sato, T.; Shoda, M. DyP, A Unique Dye-decolorizing Peroxidase Represents a Novel

Heme Peroxidase Family. Asp171 Replaces the Distal Histidine of Classical Peroxidases. *J. Biol. Chem.* **2007**, *282*, 36652–36658.

(11) Yoshida, T.; Tsuge, H.; Hisabori, T.; Sugano, Y. Crystal Structures of Dye-Decolorizing Peroxidase with Ascorbic Acid and 2,6-dimethoxyphenol. *FEBS Lett.* **2012**, *586*, 4351–4356.

(12) Sato, T.; Hara, S.; Matsui, T.; Sasaki, G.; Saijo, S.; Ganbe, T.; Tanaka, N.; Sugano, Y.; Shoda, M. A Unique Dye-decolorizing Peroxidase, DyP, from *Thanatephorus cucumeris* Dec 1: Heterologous Expression, Crystallization and Preliminary X-ray Analysis. *Acta Crystallogr., Sect. D: Biol. Crystallogr.* **2004**, *60*, 149–152.

(13) Strittmatter, E.; Liers, C.; Ullrich, R.; Wachter, S.; Hofrichter, M.; Plattner, D. A.; Piontek, K. First Crystal Structure of a Fungal High-redox Potential Dye-decolorizing Peroxidase: Substrate Interaction Sites and Long-range Electron Transfer. *J. Biol. Chem.* **2013**, *288*, 4095–4102.

(14) Liers, C.; Aranda, E.; Strittmatter, E.; Piontek, K.; Plattner, D. A.; Zorn, H.; Ullrich, R.; Hofrichter, M. Phenol Oxidation by DyP-type Peroxidases in Comparison to Fungal and Plant Peroxidases. *J. Mol. Catal. B: Enzym.* **2014**, *103*, 41–46.

(15) Linde, D.; Pogni, R.; Cañellas, M.; Lucas, F.; Guallar, V.; Baratto, M. C.; Sinicropi, A.; Sáez-Jiménez, V.; Coscolín, C.; Romero, A.; et al. Catalytic Surface Radical in Dye-decolorizing Peroxidase: a Computational, Spectroscopic and Site-directed mutagenesis study. *Biochem. J.* **2015**, *466*, 253–262.

(16) Liers, C.; Bobeth, C.; Pecyna, M.; Ullrich, R.; Hofrichter, M. DyP-like Peroxidases of the Jelly Fungus *Auricularia Auricula-judae* Oxidize Nonphenolic Lignin Model Compounds and High-redox Potential Dyes. *Appl. Microbiol. Biotechnol.* **2010**, *85*, 1869–1879.

(17) Linde, D.; Coscolín, C.; Liers, C.; Hofrichter, M.; Martínez, A. T.; Ruiz-Dueñas, F. J. Heterologous Expression and Physicochemical Characterization of a Fungal Dye-decolorizing Peroxidase From *Auricularia auricula-judae*. *Protein Expression Purif.* **2014**, *103*, 28–37.

(18) Dunford, H. B. *Heme Peroxidases*; John Wiley & Sons: New York, 1999; pp 281–308.

(19) Doyle, W. A.; Blodig, W.; Veitch, N. C.; Piontek, K.; Smith, A. T. Two Substrate Interaction Sites in Lignin Peroxidase Revealed by Site-directed Mutagenesis. *Biochemistry* **1998**, *37*, 15097–15105.

(20) Pérez-Boada, M.; Ruiz-Dueñas, F. J.; Pogni, R.; Basosi, R.; Choinowski, T.; Martínez, M. J.; Piontek, K.; Martínez, A. T. Versatile Peroxidase Oxidation of High Redox Potential Aromatic Compounds: Site-directed Mutagenesis, Spectroscopic and Crystallographic Investigations of Three Long-range Electron Transfer Pathways. *J. Mol. Biol.* **2005**, *354*, 385–402.

(21) Floudas, D.; Binder, M.; Riley, R.; Barry, K.; Blanchette, R. A.; Henrissat, B.; Martínez, A. T.; Otiillar, R.; Spatafora, J. W.; Yadav, J. S.; et al. The Paleozoic Origin of Enzymatic Lignin Decomposition Reconstructed from 31 Fungal Genomes. *Science* **2012**, *336*, 1715–1719.

(22) Strittmatter, E.; Wachter, S.; Liers, C.; Ullrich, R.; Hofrichter, M.; Plattner, D. A.; Piontek, K. Radical Formation on a Conserved Tyrosine Residue Is Crucial for DyP Activity. *Arch. Biochem. Biophys.* **2013**, *537*, 161–167.

(23) Linde, D.; Ruiz-Dueñas, F. J.; Fernandez-Fueyo, E.; Guallar, V.; Hammel, K. E.; Pogni, R.; Martínez, A. T. *Basidiomycete* DyPs: Genomic Diversity, Structural-functional Aspects, Reaction Mechanism and Environmental Significance. *Arch. Biochem. Biophys.* **2015**, *574*, 66–74.

(24) Martínez, A. T. Molecular Biology and Structure-function of lignin-degrading Heme Peroxidases. *Enzyme Microb. Technol.* **2002**, *30*, 425–444.

(25) Pogni, R.; Baratto, M. C.; Teutloff, C.; Giansanti, S.; Ruiz-Dueñas, F. J.; Choinowski, T.; Piontek, K.; Martínez, A. T.; Lenzian, F.; Basosi, R. A Tryptophan Neutral Radical in the Oxidized State of Versatile Peroxidase from *Pleurotus eryngii*: a Combined Multi-frequency EPR and DFT Study. *J. Biol. Chem.* **2006**, *281*, 9517–9526.

(26) Pogni, R.; Baratto, M. C.; Giansanti, S.; Teutloff, C.; Verdín, J.; Valderrama, B.; Lenzian, F.; Lubitz, W.; Vázquez-Duhalt, R.; Basosi, R. Tryptophan-based Radical in the Catalytic Mechanism of Versatile

Peroxidase from *Bjerkandera adusta*. *Biochemistry* **2005**, *44*, 4267–4274.

(27) Ruiz-Dueñas, F. J.; Morales, M.; García, E.; Miki, Y.; Martínez, M. J.; Martínez, A. T. Substrate Oxidation Sites in Versatile Peroxidase and other *Basidiomycete* Peroxidases. *J. Exp. Bot.* **2009**, *60*, 441–452.

(28) Ruiz-Dueñas, F. J.; Pogni, R.; Morales, M.; Giansanti, S.; Mate, M. J.; Romero, A.; Martínez, M. J.; Basosi, R.; Martínez, A. T. Protein Radicals in Fungal Versatile Peroxidase: Catalytic Tryptophan Radical in Both Compound I and Compound II and Studies on W164Y, W164H and W164S Variants. *J. Biol. Chem.* **2009**, *284*, 7986–7994.

(29) Miki, Y.; Calviño, F. R.; Pogni, R.; Giansanti, S.; Ruiz-Dueñas, F. J.; Martínez, M. J.; Basosi, R.; Romero, A.; Martínez, A. T. Crystallographic, Kinetic and Spectroscopic Study of the First Ligninolytic Peroxidase Presenting a Catalytic Tyrosine. *J. Biol. Chem.* **2011**, *286*, 15525–15534.

(30) Lardinois, O. M.; Medzihradzsky, K. F.; de Montellano, P. R. O. Spin Trapping and Protein Cross-linking of the Lactoperoxidase Protein Radical. *J. Biol. Chem.* **1999**, *274*, 35441–35448.

(31) Stoll, S.; Schweiger, A. EasySpin, A Comprehensive Software Package for Spectral Simulation and Analysis in EPR. *J. Magn. Reson.* **2006**, *178*, 42–55.

(32) Li, H.; Robertson, A. D.; Jensen, J. H. Very Fast Empirical Prediction and Rationalization of Protein pKa Values. *Proteins: Struct., Funct., Genet.* **2005**, *61*, 704–721.

(33) Humphrey, W.; Dalke, A.; Schulten, K. VMD - Visual Molecular Dynamics. *J. Mol. Graphics* **1996**, *14*, 33–38.

(34) Cornell, W. D.; Cieplak, P.; Bayly, C. I.; Gould, I. R.; Merz, K. M.; Ferguson, D. M.; Spellmeyer, D. C. A Second Generation Force Field For the Simulation of Proteins, Nucleic Acids, and Organic Molecules. *J. Am. Chem. Soc.* **1995**, *117*, 5179–5197.

(35) Wang, J.; Cieplak, P.; Kollman, P. A. How Well Does a Restrained Electrostatic Potential (RESP) Model Perform in Calculating Conformational Energies of Organic and Biological Molecules? *J. Comput. Chem.* **2000**, *21*, 1049–1074.

(36) Ponder, J. W.; Case, D. A. Force Fields For Protein Simulations. *Adv. Protein Chem.* **2003**, *66*, 27–85.

(37) Jorgensen, W. L.; Chandrasekhar, J.; Madura, J. D.; Impey, R. W.; Klein, M. L. Comparison of Simple Potential Functions for Simulating Liquid Water. *J. Chem. Phys.* **1983**, *79*, 926–935.

(38) AMBER parameter database. <http://www.pharmacy.manchester.ac.uk/bryce/amber/>.

(39) Frisch, M. J.; Trucks, G. W.; Schlegel, H. B.; Scuseria, G. E.; Robb, M. A.; Cheeseman, J. R.; Montgomery, J. A., Jr.; Vreven, T.; Kudin, K. N.; Burant, J. C.; et al. *Gaussian 03*, Revision B.04; Gaussian, Inc.: Wallingford, CT, 2004.

(40) Bernini, C.; Arezzini, E.; Basosi, R.; Sinicropi, A. In Silico Spectroscopy of Tryptophan and Tyrosine Radicals Involved in the Long-Range Electron Transfer of Cytochrome c Peroxidase. *J. Phys. Chem. B* **2014**, *118*, 9525–9537.

(41) Phillips, J. C.; Braun, R.; Wang, W.; Gumbart, J.; Tajkhorshid, E.; Villa, E.; Chipot, C.; Skeel, R. D.; Kale, L.; Schulten, K. Scalable Molecular Dynamics with NAMD. *J. Comput. Chem.* **2005**, *26*, 1781–1802.

(42) Darden, T.; York, D.; Pederson, L. Particle Mesh Ewald: An N log(N) Method for Ewald Sums in Large Systems. *J. Chem. Phys.* **1993**, *98*, 10089–10092.

(43) Aquilante, F.; De Vico, L.; Ferré, N.; Ghigo, G.; Malmqvist, P.-Å.; Neogrady, P.; Pedersen, T. B.; Pitonak, M.; Reiher, M.; Roos, B. O.; et al. MOLCAS 7: The Next Generation. *J. Comput. Chem.* **2010**, *31*, 224–247.

(44) Ponder, J. W. Tinker 4.2, software tools for molecular design; 2004. <http://dasher.wustl.edu/tinker>.

(45) Bernini, C.; Andruniów, T.; Olivucci, M.; Pogni, R.; Basosi, R.; Sinicropi, A. Effects Of The Protein Environment on the Spectral Properties of Tryptophan Radicals in *Pseudomonas aeruginosa* Azurin. *J. Am. Chem. Soc.* **2013**, *135*, 4822–4833.

(46) Bernini, C.; Pogni, R.; Ruiz-Dueñas, F. J.; Martínez, A. T.; Basosi, R.; Sinicropi, A. EPR Parameters of Amino Acid Radicals in P.

eryngii Versatile Peroxidase and Its W164Y Variant Computed at the QM/MM Level. *Phys. Chem. Chem. Phys.* **2011**, *13*, 5078–5098.

(47) Bernini, C.; Pogni, R.; Basosi, R.; Sinicropi, A. The Nature of Tryptophan Radicals Involved in the Long-range Electron Transfer of Lignin Peroxidase and Lignin Peroxidase-like Systems: Insights from Quantum Mechanical/molecular Mechanics Simulations. *Proteins: Struct., Funct., Genet.* **2012**, *80*, 1476–1485.

(48) Neese, F. *ORCA, Version 2.9, An Ab Initio, Density Functional and Semiempirical Program Package*; Max Planck-Institute for Bioinorganic Chemistry: Mülheim a.d. Ruhr, Germany, 2012.

(49) Becke, A. D. Density Functional Thermochemistry. III. The Role of Exact Exchange. *J. Chem. Phys.* **1993**, *98*, 5648–5652.

(50) Lee, C.; Yang, W.; Parr, R. G. Development of the Colle-Salvetti Correlation-Energy Formula into a Functional of the Electron Density. *Phys. Rev. B: Condens. Matter Mater. Phys.* **1988**, *37*, 785–789.

(51) Stephens, P. J.; Devlin, F. J.; Chabalowski, C. F.; Frisch, M. J. Ab Initio Calculation of Vibrational Absorption and Circular Dichroism Spectra Using Density Functional Force Fields. *J. Phys. Chem.* **1994**, *98*, 11623–11627.

(52) Barone, V. *Recent Advances in Density Functional Methods, Part I*; Chong, D. P., Ed.; World Scientific Publishing: River Edge, NJ, 1995.

(53) Bleifuss, G.; Kolberg, M.; Potsch, S.; Hofbauer, W.; Bittl, R.; Lubitz, W.; Graslund, A.; Lassmann, G.; Lenzian, F. Tryptophan and Tyrosine Radicals in Ribonucleotide Reductase: a Comparative High-field EPR Study At 94 GHz. *Biochemistry* **2001**, *40*, 15362–15368.

(54) Schünemann, V.; Lenzian, F.; Jung, C.; Contzen, J.; Barra, A. L.; Sligar, S. G.; Trautwein, A. X. Enzyme Catalysis and Regulation: Tyrosine Radical Formation in the Reaction of Wild Type and Mutant Cytochrome P450cam with Peroxy Acids: a Multifrequency EPR Study of Intermediates on the Millisecond Time Scale. *J. Biol. Chem.* **2004**, *279*, 10919–10930.

(55) Un, S. The g-Values and Hyperfine Coupling of Amino Acid Radicals in Proteins: Comparison of Experimental Measurements with Ab Initio Calculations. *Magn. Reson. Chem.* **2005**, *43*, S229–S236.

(56) Jeschke, G. EPR Techniques for Studying Radical Enzymes. *Biochim. Biophys. Acta, Bioenerg.* **2005**, *1707*, 91–102.

(57) Faller, P.; Goussias, C.; Rutherford, A. W.; Un, S. Resolving Intermediates in Biological Proton-Coupled Electron Transfer: a Tyrosyl Radical Prior to Proton Movement. *Proc. Natl. Acad. Sci. U. S. A.* **2003**, *100*, 8732–8735.

(58) Stoll, S.; Shafaat, H. S.; Krzystek, J.; Ozarowski, A.; Tauber, M. J.; Kim, J. E.; Britt, R. D. Hydrogen Bonding of Tryptophan Radicals Revealed by EPR At 700 GHz. *J. Am. Chem. Soc.* **2011**, *133*, 18098–18101.

(59) Ivancich, A.; Mattioli, T. A.; Un, S. Effect of Protein Microenvironment on Tyrosyl Radicals. A High-Field (285 GHz) EPR, Resonance Raman and Hybrid Density Functional Study. *J. Am. Chem. Soc.* **1999**, *121*, 5743–5753.

(60) Bernini, C.; Sinicropi, A.; Basosi, R.; Pogni, R. Tyrosyl Radical In the W164Y Mutant of *P. eryngii* Versatile Peroxidase: an EPR and DFT/PCM Study. *Appl. Magn. Reson.* **2010**, *37*, 279–288.

(61) Harriman, A. Further Comments on the Redox Potential of Tryptophan and Tyrosine. *J. Phys. Chem.* **1987**, *91*, 6102–6104.

(62) Smith, A. T.; Doyle, W. A.; Dorlet, P.; Ivancich, A. Spectroscopic Evidence for an Engineered, Catalytically Active Trp Radical That Creates the Unique Reactivity of Lignin Peroxidase. *Proc. Natl. Acad. Sci. U. S. A.* **2009**, *106*, 16084–16089.

(63) Hoffman, B. M.; Roberts, J. E.; Kang, C. H.; Margoliash, E. Electron Paramagnetic and Electron Nuclear Double Resonance of the Hydrogen Peroxide Compound of Cytochrome c Peroxidase. *J. Biol. Chem.* **1981**, *256*, 6556–6564.

(64) Sivaraja, M.; Goodin, D. B.; Smith, M.; Hoffman, B. M. Identification by ENDOR of Trp191 as the Free-Radical Site in Cytochrome c Peroxidase Compound ES. *Science* **1989**, *245*, 738–740.

(65) Huyett, J. E.; Doan, P. E.; Gurbiel, R.; Houseman, A. L. P.; Sivaraja, M.; Goodin, D. B.; Hoffman, B. M. Compound ES of Cytochrome c Peroxidase Contains a Trp π -Cation Radical: Characterization by CW and Pulsed Q-Band ENDOR Spectroscopy. *J. Am. Chem. Soc.* **1995**, *117*, 9033–9041.

(66) Liu, R. Q.; Miller, M. A.; Han, G. W.; Hahn, S.; Geren, L.; Hibdon, S.; Kraut, J.; Durham, B.; Millet, F. Role of Methionine 230 in Intramolecular Electron Transfer Between the Oxyferryl Heme and Tryptophan 191 in Cytochrome c Peroxidase Compound II. *Biochemistry* **1994**, *33*, 8678–8685.

(67) Jensen, G. M.; Bunte, S. W.; Warshel, A.; Goodin, D. B. Energetics of Cation Radical Formation at the Proximal Active Site Tryptophan of Cytochrome c Peroxidase and Ascorbate Peroxidase. *J. Phys. Chem. B* **1998**, *102*, 8221–8228.

(68) Barrows, T. P.; Bhaskar, B.; Poulos, T. L. Electrostatic Control of the Tryptophan Radical in Cytochrome c Peroxidase. *Biochemistry* **2004**, *43*, 8826–8834.